Electronic Supplementary Information

Spontaneous unbinding transition of nanoparticles adsorbing onto biomembranes: interplay of electrostatics and crowding

Anurag Chaudhury[#], Koushik Debnath[$], Nikhil R. Jana[$], and Jaydeep K. Basu[#†]

#Department of Physics, Indian Institute of Science, Bangalore 560012, India

$School of Materials Science, Indian Association for the Cultivation of Sciences, Kolkata 700032, India

†E-mail: basu@iisc.ac.in

Phone: +91-80-2293 3281

Nanoparticle Synthesis and Characterization:

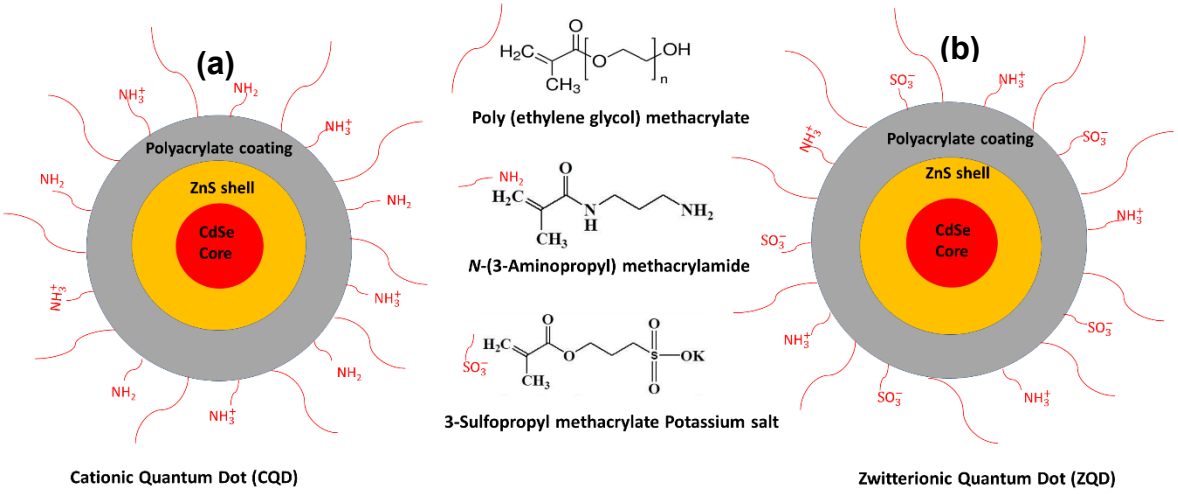

Fig. S1: Schematic of a) CQD and b) ZQD

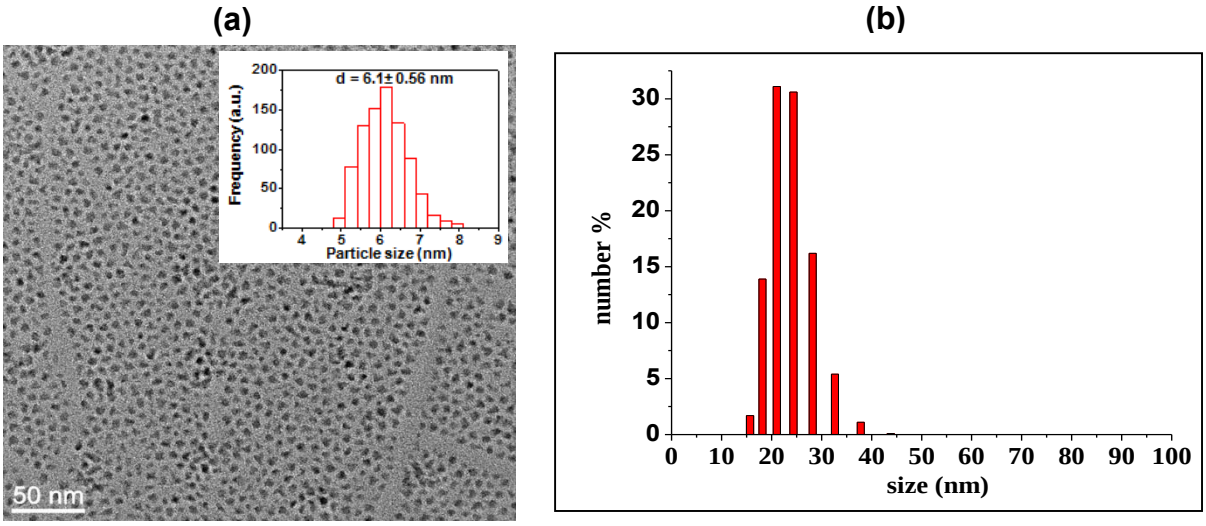

Fig. S2: a) TEM image of QD (inset shows quantified diameter of the CdSe/ZnS Core/shell), b) Hydrodynamic size distribution of QDs

Red emissive quantum dots (QDs) having CdSe core and ZnS shell have been synthesized by previously reported method [1,2]. Briefly speaking, first of all, the CdSe nanocrystals were synthesized in octadecane solution at 280^0C followed by the ZnS shelling on these nanoparticles at 200°C. These hydrophobic quantum dots were then transformed into hydrophilic via polyacrylate coating by using N-(3-aminopropyl) methacrylamide, poly (ethyleneglycol) methacrylate and bis[2-(methacryloyloxy)ethyl] phosphate as acrylate monomers.

In this work, we used Cationic (CQD) and Zwitterionic (ZQD) Quantum Dots. The composition and structure of the QDs have been shown in Fig. S1.

These quantum dots were characterized for their size and surface charge. For measuring diameter of CdSe/ZnS core-shell transmission electron microscope (TEM) images were recorded using Technai G2 T20 microscope at an accelerating voltage of 200 kV. Aqueous solution of quantum dots were deposited on carbon coated copper mesh grid and dried properly before imaging. The diameter of the semiconductor core of the quantum dots was found to be 6.1 ± 0.56 nm (Fig. S2 a).

The zeta potential and hydrodynamic diameter were measured using a Zetasizer Nano ZS (Malvern Instruments, U.K.). The instrument uses a 2 mW He-Ne laser of wavelength 633 nm to illuminate the sample. A disposable zeta cuvette was used for both size and zeta potential measurements. In DLS, back-scattered light at an angle of 173^0 was detected and fed to the digital signal processing correlator. To perform the measurements, PBS buffer solution of pH 7 was used. For the sample preparation typically quantum dots solutions are dispersed in different buffer solutions maintaining the final concentration of 1 µM. Hydrodynamic diameter of both the CQD and ZQD and were found to be 21 ± 0.15 nm (Fig. S2 b). The zeta potential of CQD and ZQD were measured to be +18 ± 1 mV and +0.9 ± 1 mV respectively at pH 7.

The Absorption and Emission spectra of these QDs have been shown in Fig. S3.

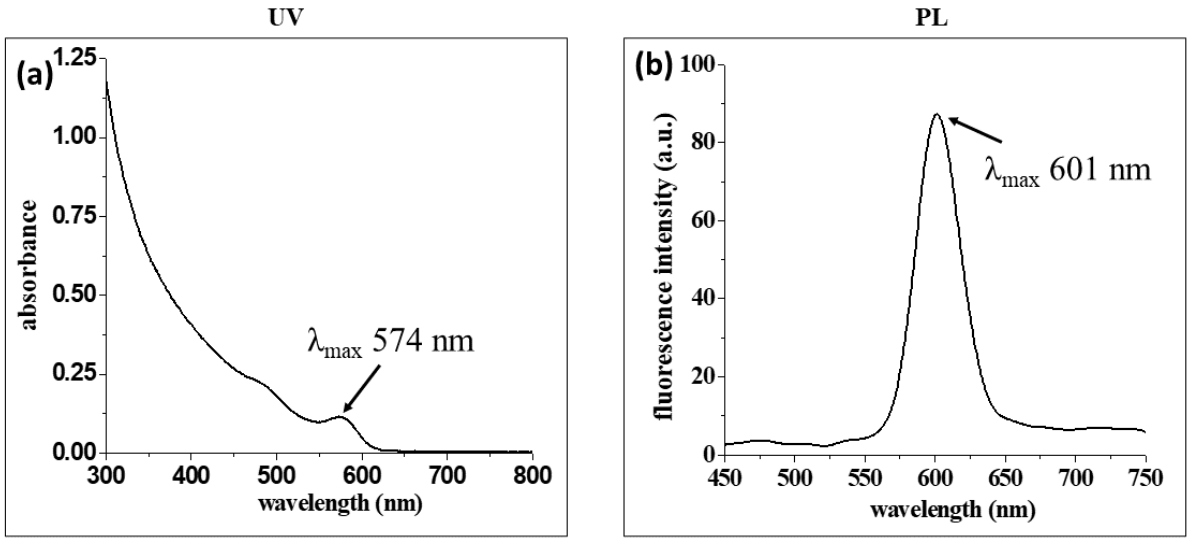

Fig. S3: a) Absorption spectrum of the QDs, b) Photoluminescence spectrum of the QDs

Isotherms of Langmuir monolayers:

The isotherm data were collected in the manner described in the Materials and Methods section of the article. The FLMs were compressed and expanded once before the final compression, in order to form a homogeneous film at the air-water interface. The isothermal compression modulus (β) of the lipid monolayer was calculated by using the equation,

$$\beta = -A\left(\frac{\partial \pi}{\partial A}\right)_T$$

where, π and A are the measured surface pressure and area of the monolayer, respectively, at a constant temperature, T= 20^{0}C. The parameter $(\partial\pi/\partial A)_T$ was calculated by differentiating the pressure-area isotherm. The isothermal compression modulus is used to describe mechanical properties of these monolayers. In addition, higher β value suggests the formation of condensed well-packed monolayer. From the β plots, it is observed that the compression modulus of pristine P1G1 monolayer is much higher than O1G1 suggesting that P1G1 is a much highly packed monolayer. The isotherms after adding QDs show a higher surface pressure indicating the binding of the QDs and increasing the membrane tension.

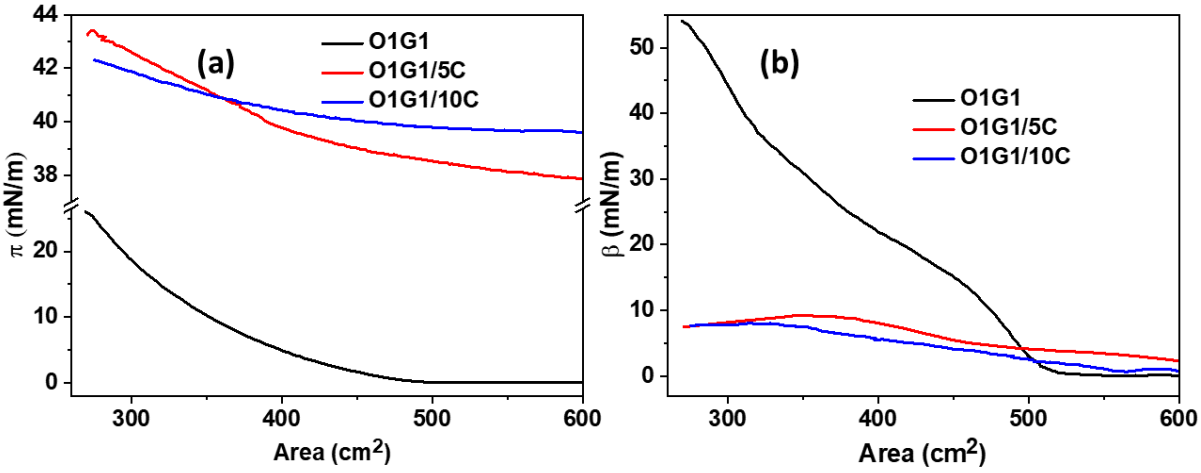

Fig. S4: (a) Langmuir isotherms (plotting surface pressure, π) and (b) Isothermal compression modulus (β) of O1G1, O1G1 + 5nM CQD (O1G1/5C) and O1G1 + 10 nM CQD (O1G1/10C).

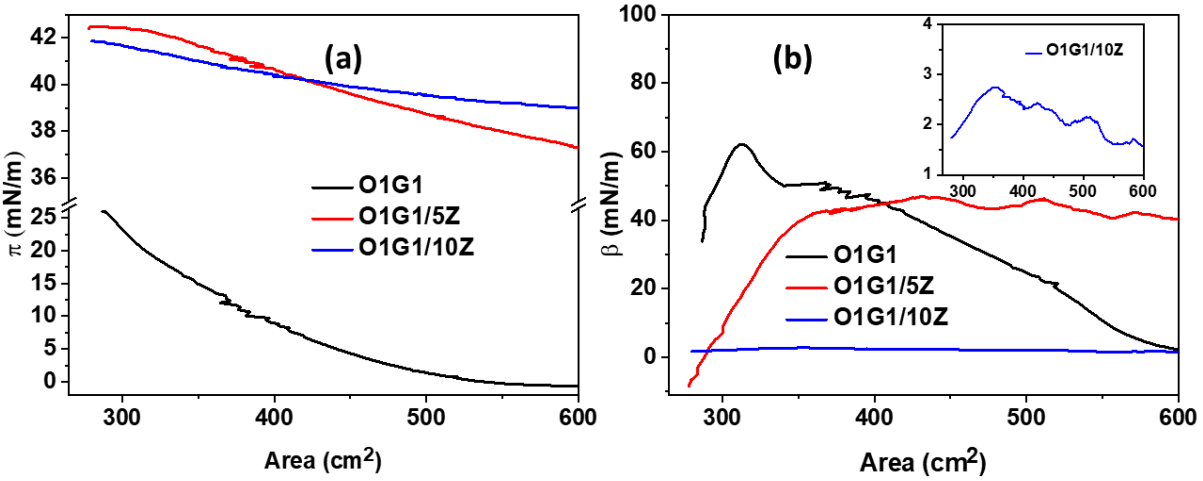

Fig. S5: (a) Langmuir isotherms (plotting surface pressure, π) and (b) Isothermal compression modulus (β) of O1G1, O1G1 + 5nM ZQD (O1G1/5Z) and O1G1 + 10 nM ZQD (O1G1/10Z). The inset of b shows the plot of O1G1/10Z clearly in a reduced scale along the y-axis.

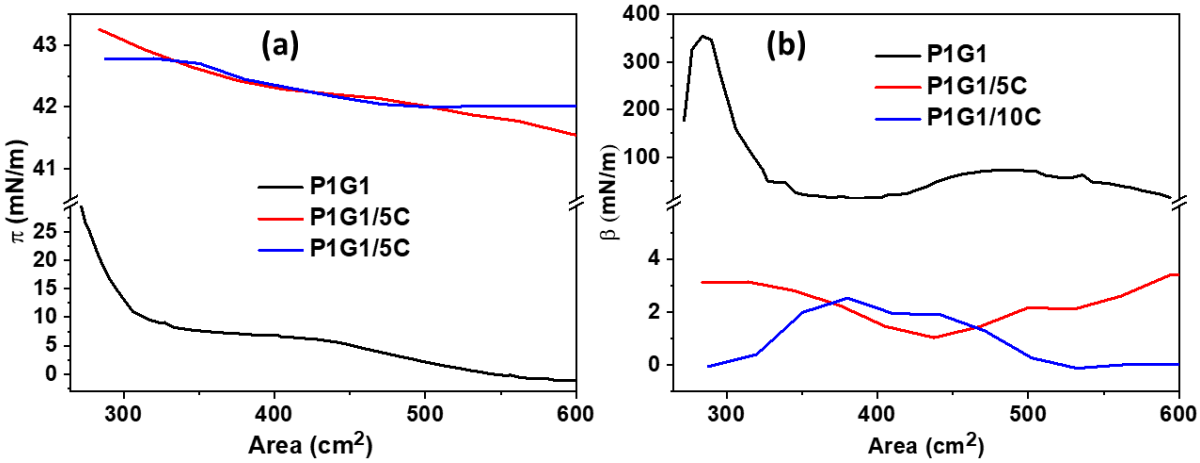

Fig. S6: (a) Langmuir isotherms (plotting surface pressure, π) and (b) Isothermal compression modulus (β) of P1G1, P1G1 + 5nM CQD (P1G1/5C) and P1G1 + 10 nM CQD (P1G1/10C).

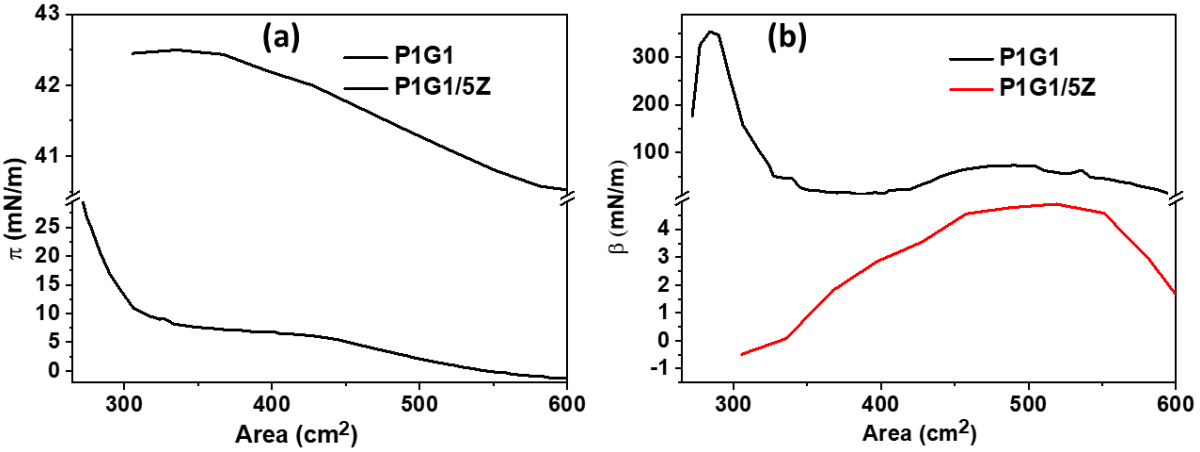

Fig. S7: (a) Langmuir isotherms (plotting surface pressure, π) and (b) Isothermal compression modulus (β) of P1G1 and P1G1 + 5nM ZQD (P1G1/5Z)

Neutron Reflectivity data:

The NR profiles were collected for pristine O1G1 and P1G1 monolayers as well as their profiles after adding CQDs and ZQDs in the subphase. The parameters extracted out of the data collected from the pristine FLMs present above two contrast subphases have been listed in Table S1 below. To obtain the error bar for each parameter in a particular data, at first, the NR data was fitted to get the best possible fit; thereafter, all the other parameters were constrained and the NR dataset was allowed to fit with 200 iterations with a certain reasonable range

for the concerned parameter. MOTOFIT provides the error bar for that parameter around the best fitted value. The D_2O contrast and the NRW contrast NR profiles were tried to be fitted in a co-refined (simultaneously) manner. Fig. S8 shows the fits. It can be seen that the D_2O contrast profile fit was compromised as well as there is misfit in the low q_z region of the NRW contrast profile in the process of obtaining satisfactory fits for both. D_2O contrast obviously has more features. Therefore, NR fit for the D_2O contrast data was fit first. Thereafter, the NRW NR profile was fitted by constraining the thicknesses of the head and tail layers to those obtained from the corresponding D_2O contrast fit. P1G1, being a more packed FLM, its thickness was found to be more than that of O1G1. Also, the water penetration into the P1G1 monolayer was relatively less as it is a more packed system (Table S1).

Table S1: Fit parameters of pristine O1G1 (at 26mN/m and 20^0C) and P1G1 (at 26mN/m and 20^0C) and water content in the layers

Layer	**t (Å)**	**ρ (x 10^{-6} Å^{-2})**	**iρ (x 10^{-14} Å^{-2})**	**σ (Å)**	**ϕ_w (%)**
O1G1/Tail in D_2O	16.7 ± 0.1	2.01 ± 0.01	-1.07 ± 0.88	7.0 ± 0.2	10.7 ± 0.1
O1G1/Head in D_2O	7.0 ± 0.1	2.32 ± 0.10	-167.34 ± 1.65	3.0 ± 0.4	20.6 ± 1.0
D_2O	infinity	5.90 ± 0.00	-13.20 ± 0.13	5.0 ± 0.1	100
O1G1/Tail in NRW	16.7*	1.38 ± 0.01	-100.00 ± 0.85	1*	10.7 ± 0.1
O1G1/Head in NRW	7.0*	1.10 ± 0.02	-112.90 ± 3.81	1*	20.6 ± 1.0
NRW	infinity	0.00 ± 0.00	-10.00 ± 0.35	1*	100
P1G1/ Tail in D_2O	16.48 ± 0.1	5.45 ± 0.03	-55.76 ± 0.80	5.0 ± 0.1	0
P1G1/ Head in D_2O	8.8± 0.0	2.29 ± 0.02	-20.48 ± 1.55	1.6 ± 0.3	14.4 ± 0.2
D_2O	infinity	5.95 ± 0.00	-12.92 ± 0.13	4.8 ± 0.2	100
P1G1/ Tail in NRW	16.4*	5.66 ± 0.00	-10.12 ± 3.84	1.0 ± 0.2	0
P1G1/ Head in NRW	8.8*	1.43 ± 0.01	-37.08 ± 1.71	1.0 ± 0.4	14.4 ± 0.2
NRW	infinity	0.00 ± 0.01	-10.53 ± 0.27	6.0 ± 0.2	100

*Values were fixed while fitting.

t=thickness of the layer

ρ=Real part of the SLD

iρ=Imaginary part of the SLD

σ=roughness of the layer at the interface with the adjacent layer above it

ϕ_w=fraction of water content in the layer

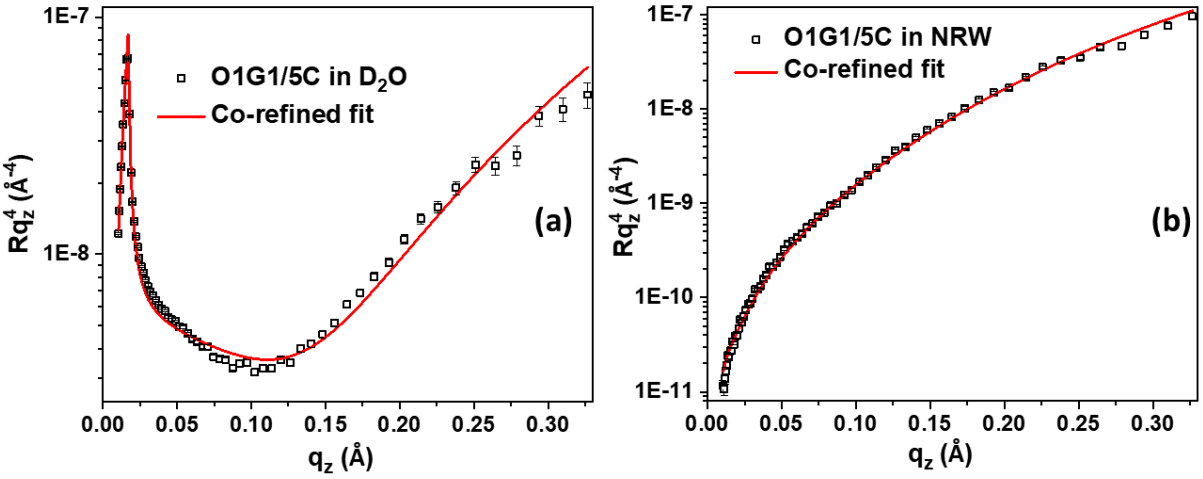

Fig S8: shows the NR Rq_Z^4 profile of DOPC:DPPG/1/1 + 5 nM CQD (O1G1/5C) collected on a) D_2O subphase and b) Null Reflecting Water (NRW) subphase. Both the profiles were fitted simultaneously in a co-refined manner, and the red solid line in each panel shows their fits. The profiles were fitted with a 3 layer model consisting a lipid tail, lipid head and a CQD layer beneath.

Fig. S9 shows a 2-layer fit as well as a 3-layer fit for the O1G1/5C system collected on D_2O subphase. A numerical parameter called the reduced chi squared value, χ^2 was used to quantify the goodness of the fit. χ^2 is defined as follows:-

$$\chi^2 = \sum_{n=1}^{L} \frac{1}{L-P} \left(\frac{y_{n,obs} - y_{n,cal}}{y_{n,error}} \right)^2$$

Here, L is the number of data points in the NR profile, P is the number of parameters for the fit. $y_{n,obs}$, $y_{n,cal}$ and $y_{n,error}$ are the observed (actual data point), calculated (value obtained from the fit) and the instrumental error values of n^{th} data point in the NR profile. In Fig. S9, the fit as well as the χ^2 parameter proves that a third layer beneath the O1G1 FLM is needed to fit the profile. And the fit improves after adding the CQD layer beneath the FLM. Table S2 shows that the CQD layer at the interface with its adjacent lipid head layer above had a high roughness. This might be because the CQD core/shell was not in direct contact with the head layer rather the ligands of the CQD might be forming a layer of inconsistent thickness between the lipid headgroups and the CQD core/shell. Similar model was found to fit for all the profiles thereafter. Some of the roughness values shown in the table were quite insensitive to the fit, hence those values were fixed while fitting. Similarly, for O1G1/10C, O1G1/5Z and O1G1/10Z, 3-layer model was used to fit the NR profiles. The NR profiles collected in D_2O subphase had more features in their reflectivity profiles compared to those collected on NRW subphase. That is why, the NR profiles collected on D_2O subphase were used to show the necessity of the 3^{rd} layer for a good fit. Fig. S9,10,12,13 show the comparative fits using 2-layer and 3-layer fits and thereby justifies the need for the 3^{rd} layer.

Table S2: Fit parameters for the best fit of O1G1 + 5 nM CQD

Layer	**t (Å)**	**ρ (x 10^{-6} Å^{-2})**	**Relative QD SLD**	**iρ (x 10^{-14} Å^{-2})**	**σ (Å)**
Tail in D_2O	15.5 ± 0.1	1.61 ± 0.01	----------	-44.99 ± 1.08	2.3 ± 0.6
Tail in NRW	15.5*	1.40 ± 0.02	----------	-90.00 ± 0.78	1.0*
Head in D_2O	7.1 ± 0.0	2.44 ± 0.02	----------	-621.09 ± 1.35	2.3 ± 0.1
Head in NRW	7.1*	0.80 ± 0.01	----------	-41.24 ± 1.61	1.0*
CQD in D_2O	68.0 ± 0.4	5.19 ± 0.00	0.868	-13.08 ± 0.16	23.8 ± 0.1
CQD in NRW	68.0*	0.20 ± 0.00	0.20	-44.78 ± 0.91	27.7 ± 0.6
D_2O	Infinity	5.98 ± 0.00	----------	-25.52 ± 0.08	95.7 ± 0.4
NRW	Infinity	0.00 ± 0.02	----------	-46.88 ± 1.29	98.0 ± 5.0

t=thickness of the layer

ρ=Real part of the SLD

iρ=Imaginary part of the SLD

σ=roughness of the layer at the interface with the adjacent layer above it

ρ_{QD}= SLD of the QD layer

ρ_{SUB}= SLD of the subphase

Relative QD SLD= ρ_{QD}/ ρ_{SUB} (in case of D_2O subphase)

Relative QD SLD= ρ_{QD} - ρ_{SUB} (in case of NRW subphase)

*These values were fixed while fitting

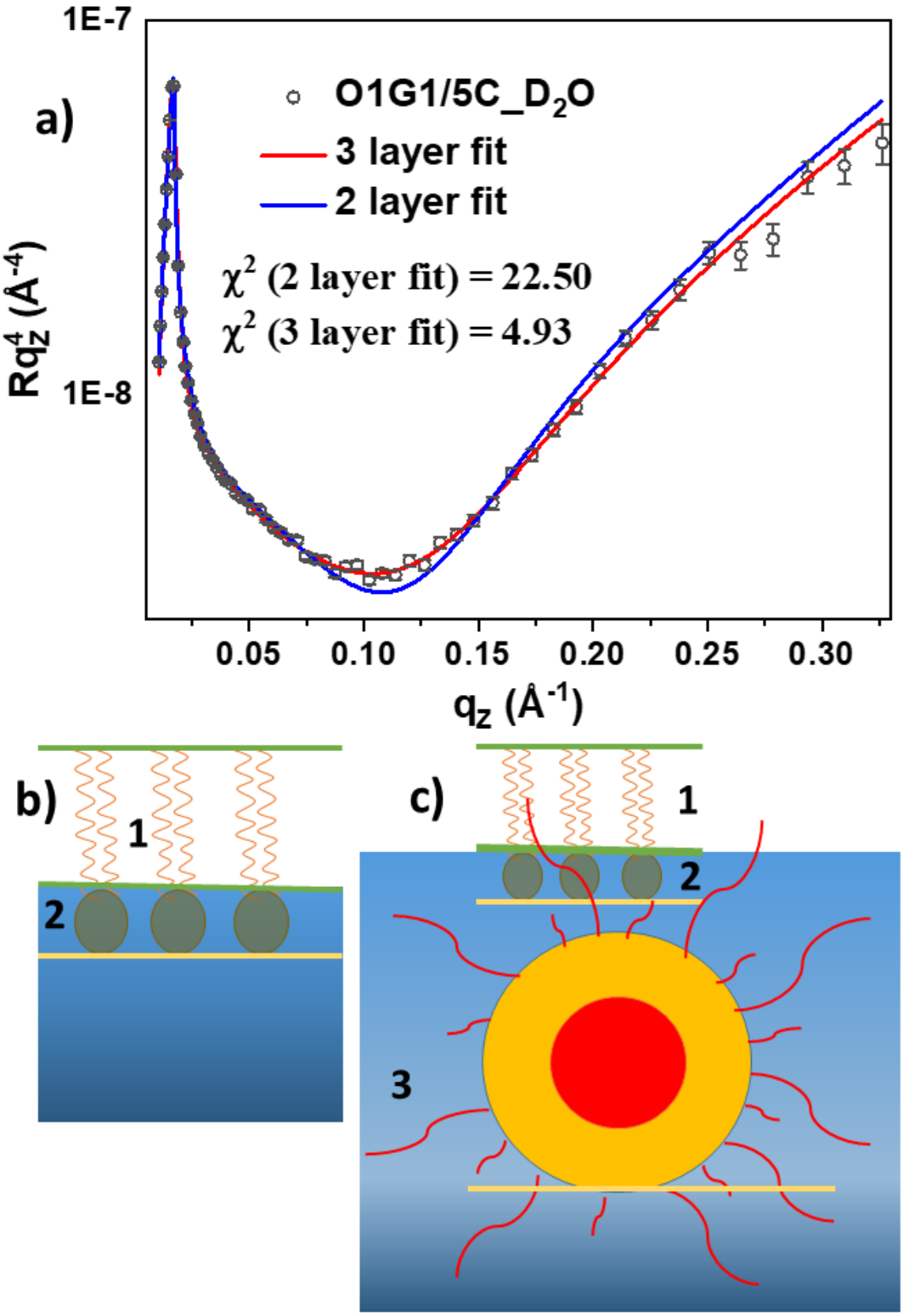

Fig S9: a) NR Rq_z^4 profile of DOPC:DPPG/1/1 (O1G1) after adding 5 nM CQD (O1G1/5C) in the D_2O subphase. The plot shows the best fit (red line) with a 3-layer model and an alternative fit (blue line) with only 2 layers. Panel b) shows the 2-layer model with lipid tail (layer 1) and head (layer 2). Panel c) shows the 3-layer model with lipid tail (layer 1), head (layer 2) and the CQD CdSe/ZnS core/shell as the layer 3. The reduced chi squared (χ^2) depicting the goodness of the respective fits are displayed on the graphs.

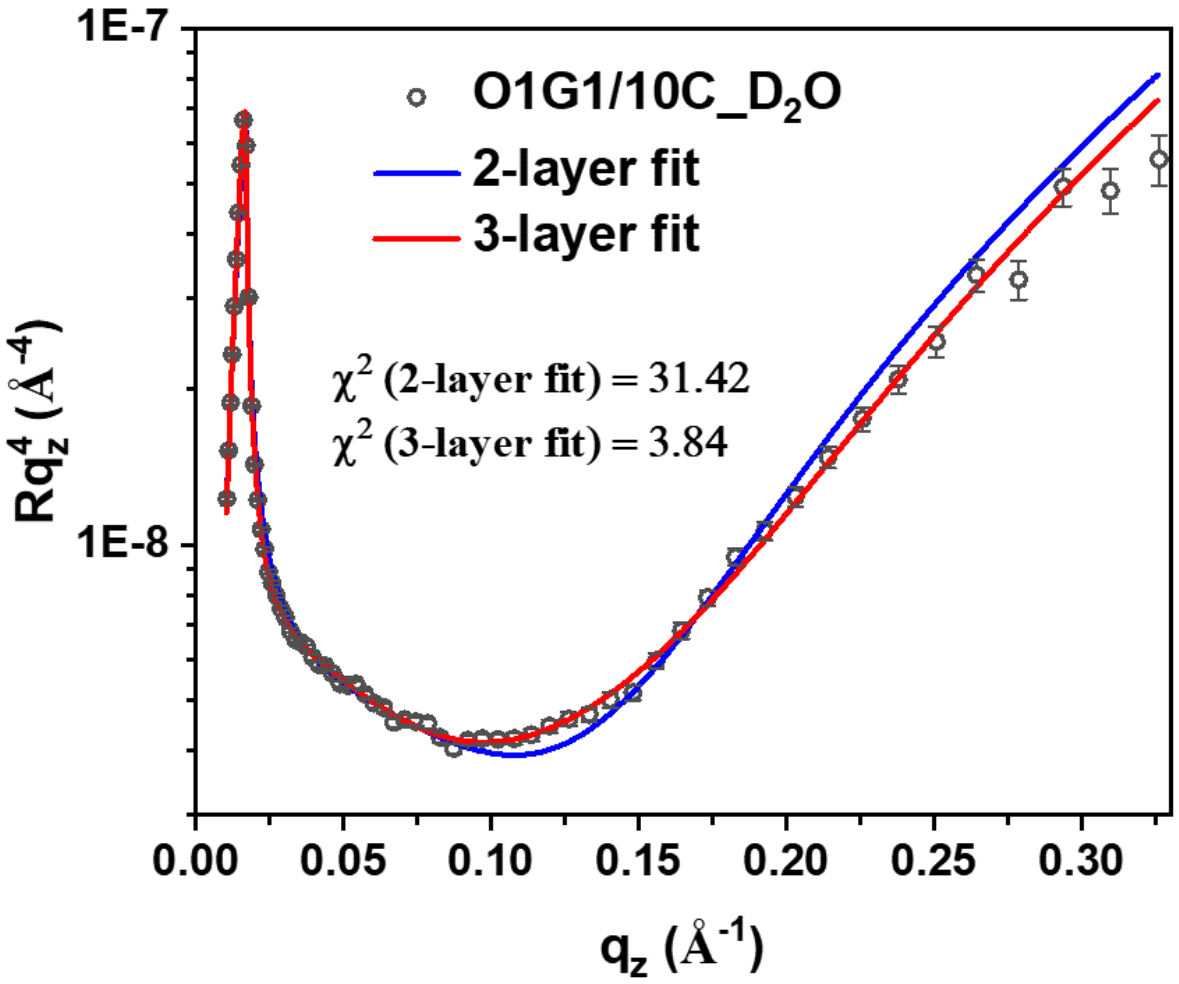

Fig S10: NR Rq_Z^4 profile of DOPC:DPPG/1/1 (O1G1) after adding 5 nM CQD (O1G1/5C) in the D_2O subphase. The plot shows the fit (blue line) with a 2-layer model and the best fit (red line) with 3 layers. The models have been illustrated in panels b), c) of Fig. S9. The reduced chi squared (χ^2) parameter depicting the goodness of the respective fits are displayed on the graphs.

Table S3: Fit parameters for the best fit of O1G1 + 10 nM CQD

Layer	t (Å)	ρ (x 10^{-6} Å^{-2})	Relative QD SLD	iρ (x 10^{-14} Å^{-2})	σ (Å)
Tail in D_2O	15.6 ± 0.1	1.46 ± 0.04	----------	-211.26 ± 0.81	4.3 ± 0.2
Tail in NRW	15.6*	0.65 ± 0.01	----------	-1.21 ± 0.99	5.0 ± 1.2
Head in D_2O	6.7 ± 0.4	3.29 ± 0.02	----------	-91.48 ± 2.08	1.2 ± 0.6
Head in NRW	6.7*	1.20 ± 0.07	----------	-406.12 ± 1.79	1.4 ± 0.5
CQD in D_2O	73.9 ± 0.7	5.14 ± 0.00	0.891	-9.83 ± 0.15	21.3 ± 0.2
CQD in NRW	73.9*	0.12 ± 0.00	0.12	-39.314 ± 0.66	11.7 ± 0.2
D_2O	Infinity	5.77 ± 0.00	----------	-15.58 ± 0.07	89.9 ± 0.8
NRW	Infinity	0.00 ± 0.01	----------	-47.70 ± 1.05	76.8 ± 3.6

t=thickness of the layer
ρ=Real part of the SLD
iρ=Imaginary part of the SLD
σ=roughness of the layer at the interface with the adjacent layer above it
ρ_{QD}= SLD of the QD layer
ρ_{SUB}= SLD of the subphase
Relative QD SLD= ρ_{QD}/ ρ_{SUB} (in case of D_2O subphase)
Relative QD SLD= ρ_{QD} - ρ_{SUB} (in case of NRW subphase)
*These values were fixed while fitting

The unhydrated SLD of the QD is around 1-1.5, which is more than the SLD of NRW but less than that of D_2O. From the relative SLD of the QD from Tables S2, S3, it is clear that the bound QD coverage, with the C_{SUB} going from 5 to 10 nM, is decreasing because in NRW subphase, the SLD of the QD layer is decreasing whilst in D_2O subphase, the SLD of the QD layer is increasing, indicative of lower QD coverage and more D_2O content in the layer.

For O1G1/5Z and O1G1/10Z, the trend is just reverse, as can be quantified from the relative QD SLD values in Tables S4, S5.

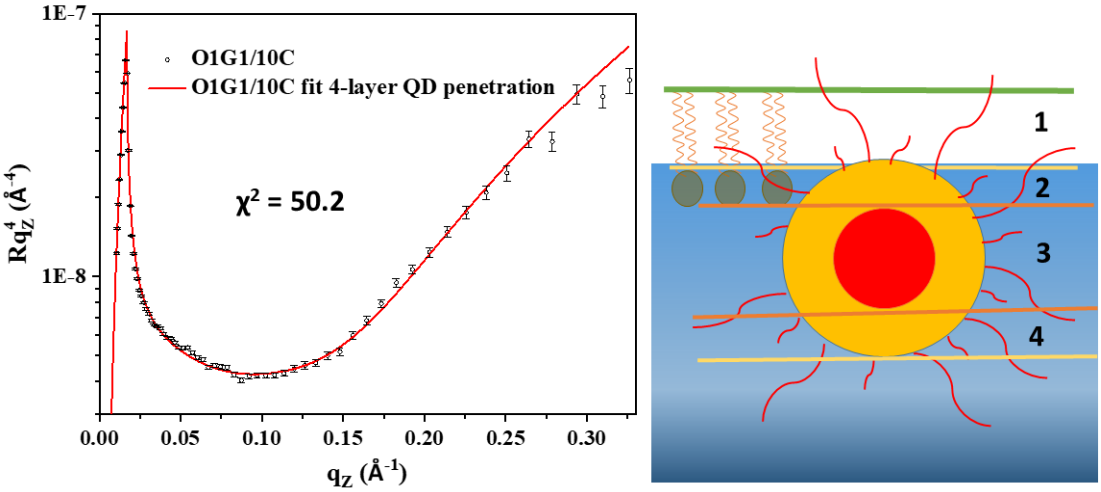

Fig S11: The left panel shows the fit of the O1G1/10C data collected in the D_2O subphase using a 4-layer model where the CQD has penetrated the monolayer. The corresponding schematic of the model is shown in the right panel.

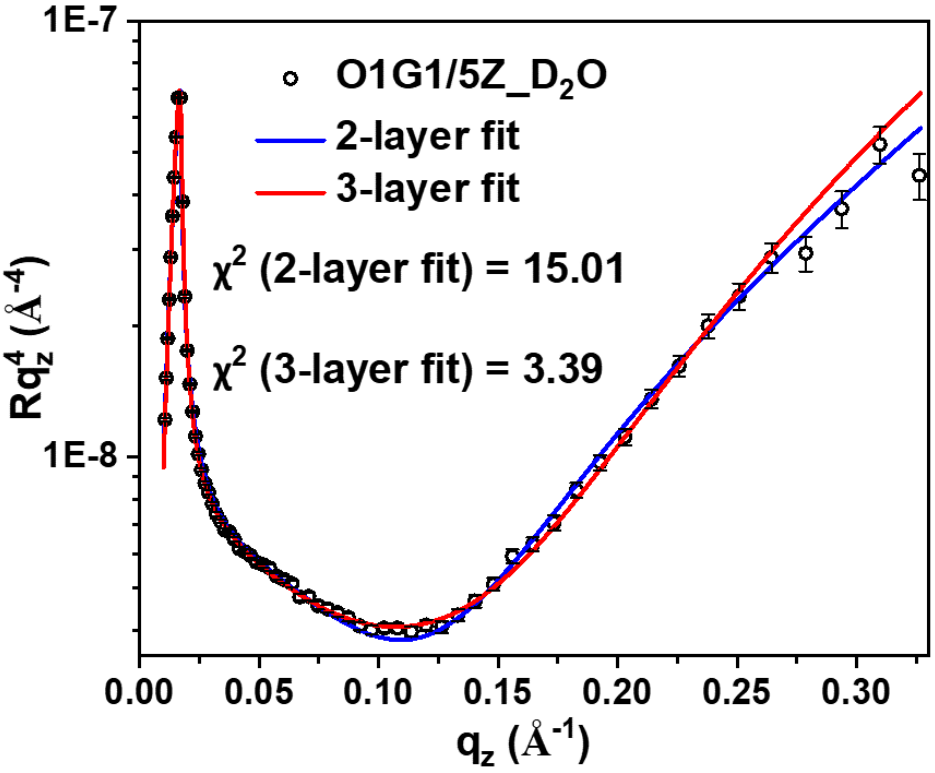

Fig S12: NR Rq_z^4 profile of DOPC:DPPG/1/1 (O1G1) after adding 5 nM ZQD (O1G1/5Z) in the D_2O subphase. The plot shows the fit (blue line) with a 2-layer model and the best fit (red line) with 3 layers. The models are similar to those illustrated in panels b), c) of Fig. S9. The reduced chi squared (χ^2) depicting the goodness of the respective fits are displayed on the graphs.

Table S4: Fit parameters for the best fit of O1G1 + 5 nM ZQD

Layer	**t (Å)**	**ρ (x 10^{-6} Å^{-2})**	**Relative QD SLD**	**iρ (x 10^{-14} Å^{-2})**	**σ (Å)**
Tail in D_2O	12.0 ± 0.1	1.03 ± 0.02	----------	-231.12 ± 1.33	5.7 ± 0.2
Tail in NRW	12.0*	0.60 ± 0.02	----------	-100.00 ± 1.19	1.0*
Head in D_2O	6.4 ± 0.0	3.28 ± 0.01	----------	-396.22 ± 1.74	1.5 ± 0.4
Head in NRW	6.4*	1.20 ± 0.02	----------	-3.84 ± 3.12	1.0*
ZQD in D_2O	57.3 ± 0.4	5.25 ± 0.01	0.879	-9.81 ± 0.18	30.9 ± 0.1
ZQD in NRW	57.3*	0.16 ± 0.00	0.16	-10.00 ± 0.75	3.0 ± 1.7
D_2O	Infinity	5.97 ± 0.00	----------	-25.92 ± 0.08	97.2 ± 0.4
NRW	Infinity	0.00 ± 0.01	----------	-10.00 ± 0.56	50.0 ± 3.7

t=thickness of the layer
ρ=Real part of the SLD
iρ=Imaginary part of the SLD
σ=roughness of the layer at the interface with the adjacent layer above it
ρ_{QD}= SLD of the QD layer
ρ_{SUB}= SLD of the subphase
Relative QD SLD= ρ_{QD}/ ρ_{SUB} (in case of D_2O subphase)
Relative QD SLD= ρ_{QD} - ρ_{SUB} (in case of NRW subphase)
*These values were fixed while fitting

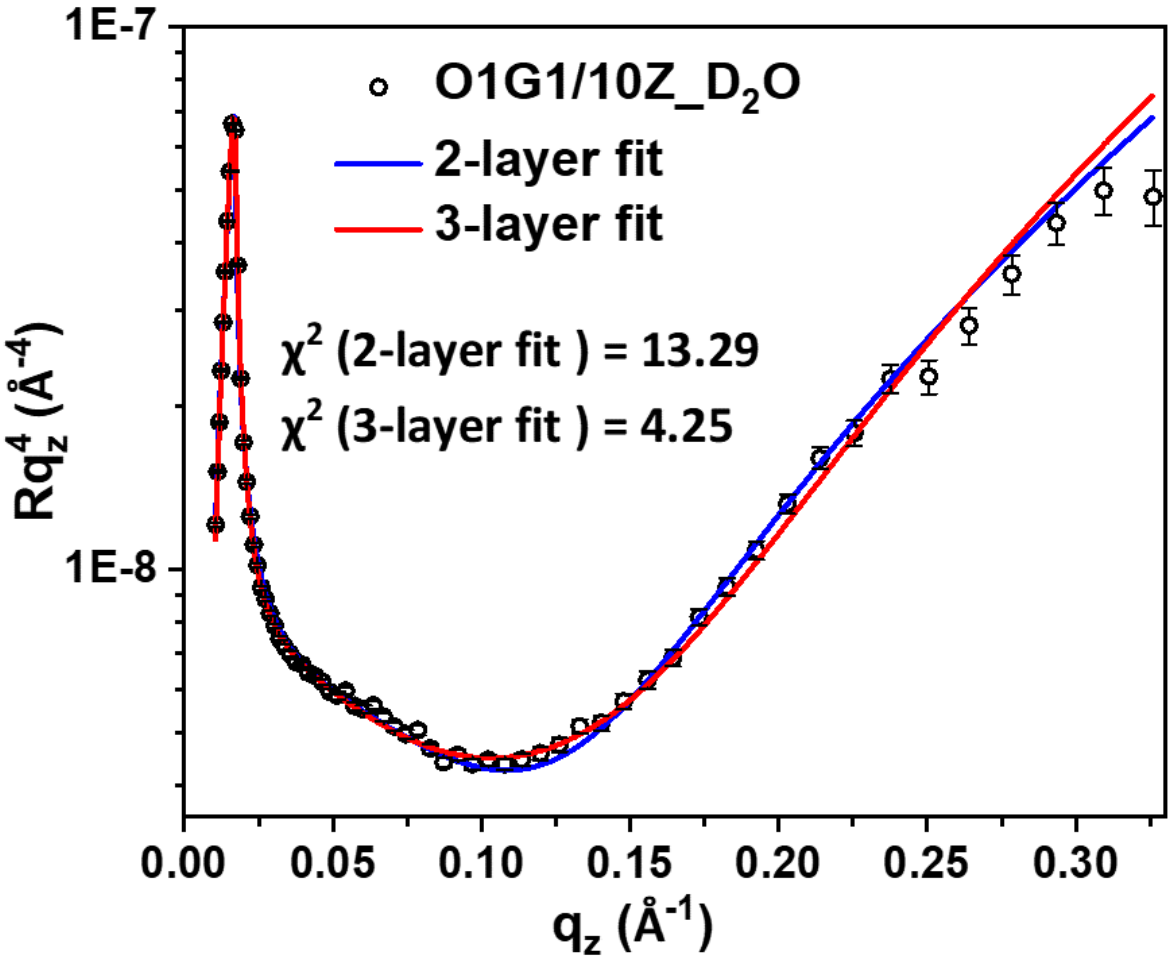

Fig S13: NR Rq_Z^4 profile of DOPC:DPPG/1/1 (O1G1) after adding 10 nM ZQD (O1G1/10Z) in the D_2O subphase. The plot shows the fit (blue line) with a 2-layer model and the best fit (red line) with 3 layers. The models are similar to those illustrated in panels b), c) of Fig. S9. The reduced chi squared (χ^2) depicting the goodness of the respective fits are displayed on the graphs.

Table S5: Fit parameters for the best fit of O1G1 + 10 nM ZQD

Layer	**t (Å)**	**ρ (x 10^{-6} Å^{-2})**	**Relative QD SLD**	**iρ (x 10^{-14} Å^{-2})**	**σ (Å)**
Tail in D_2O	12.4 ± 0.1	1.10 ± 0.02	----------	-294.34 ± 1.26	3.0 ± 0.2
Tail in NRW	12.4*	0.60 ± 0.04	----------	-99.44 ± 1.34	1.0*
Head in D_2O	6.6 ± 0.0	2.74 ± 0.01	----------	-449.14 ± 1.70	1.5 ± 0.5
Head in NRW	6.6*	0.81 ± 0.04	----------	-2.70 ± 3.05	1.0*
ZQD in D_2O	59.8 ± 0.3	5.08 ± 0.01	0.859	-2.28 ± 0.21	30.9 ± 0.1
ZQD in NRW	59.8*	0.17 ± 0.01	0.17	-28.32 ± 0.83	3.0 ± 2.0
D_2O	Infinity	5.91 ± 0.00	----------	-27.76 ± 0.09	86.4 ± 0.4
NRW	Infinity	0.00 ± 0.00	----------	-51.54 ± 2.87	98.9 ± 3.1

t=thickness of the layer
ρ=Real part of the SLD
iρ=Imaginary part of the SLD
σ=roughness of the layer at the interface with the adjacent layer above it
ρ_{QD}= SLD of the QD layer
ρ_{SUB}= SLD of the subphase
Relative QD SLD= ρ_{QD}/ ρ_{SUB} (in case of D_2O subphase)
Relative QD SLD= ρ_{QD} - ρ_{SUB} (in case of NRW subphase)
*These values were fixed while fitting

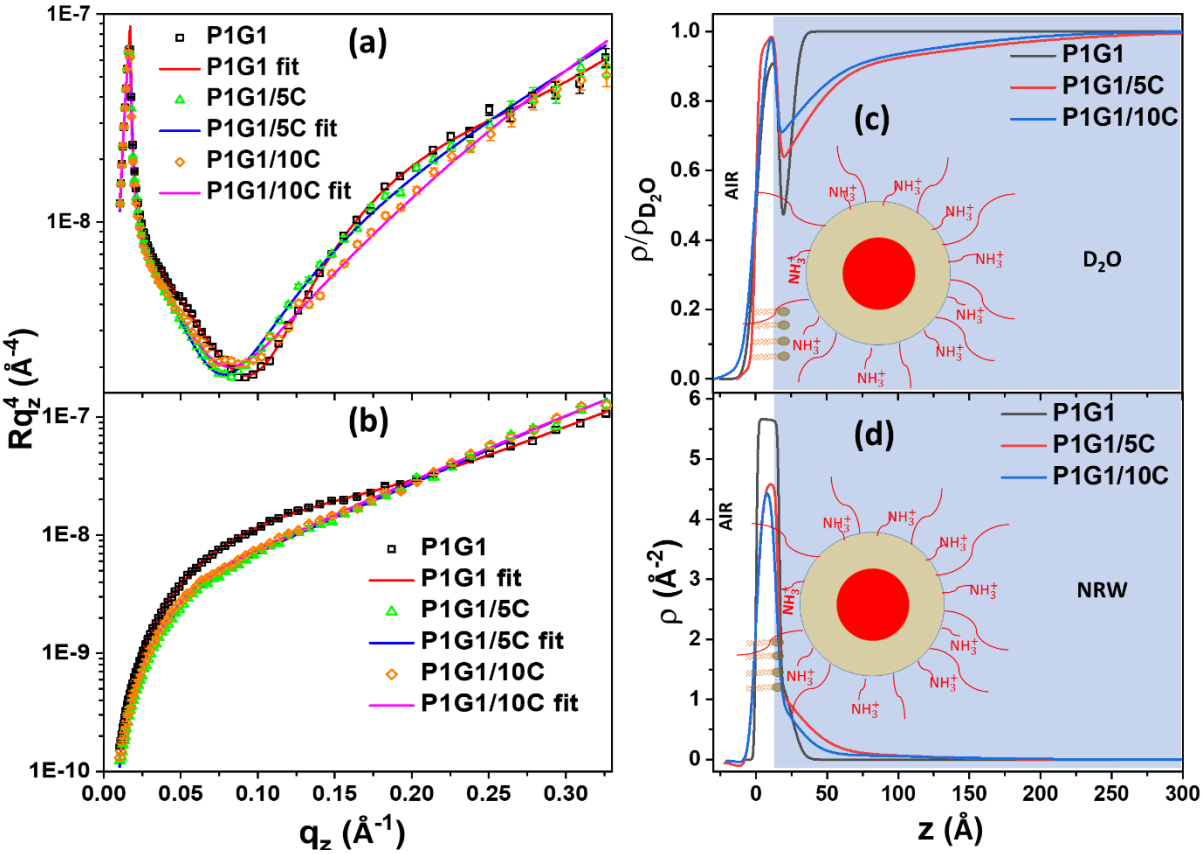

Fig S14: NR Rq_z^4 profile of pristine d_{62}-DPPC:DPPG/1/1 (P1G1) , P1G1 after adding 5 nM CQD (P1G1/5C) and 10 nM CQD (P1G1/10C) in the (a) D_2O subphase and (b) in the null reflecting water (NRW) subphase. (c) shows the normalised scattering length density profiles (ρ/ρ_{D_2O}) of the NR profiles shown in a). (d) shows the scattering length density profiles of the NR profiles shown in b).

The qualitative changes of CQD binding which were observed for O1G1 FLMs (discussed in the main manuscript) were also observed for P1G1 FLMs. Fig. S14a shows that the NR profiles of P1G1 after adding CQDs shifted to lower q_z values indicating the layer getting thicker. Changes are also clear from the profiles collected in NRW subphase (Fig. S14b). Fitting the NR profiles of P1G1 after CQD addition with a 3rd layer gives the best fit. P1G1/5C (P1G1 + 5 nM CQD) reveals a more CQD coverage than P1G1/10C. This is similar to the observation noted for

O1G1 FLMs. P1G1/5C gives a CQD coverage of 19.6 ± 1.2%, whereas P1G1/10C has a coverage of 17.9 ± 1.2%. The SLD of the QD layer relative to the subphase shows the decrement in bound CQD coverage as the subphase concentration was increased from 5 to 10 nM (Tables S6, S7).

Table S6: Fit parameters for the best fit of P1G1 + 5 nM CQD

Layer	**t (Å)**	**ρ (x 10^{-6} Å^{-2})**	**Relative QD SLD**	**iρ (x 10^{-14} Å^{-2})**	**σ (Å)**
Tail in D_2O	15.6 ± 0.1	4.79 ± 0.02	----------	-242.26 ± 0.87	2.0 ± 0.1
Tail in NRW	15.6*	5.13 ± 0.02	----------	-70.22 ± 1.85	4.3 ± 0.1
Head in D_2O	7.0 ± 0.1	2.51 ± 0.01	----------	-365.46 ± 1.57	1.9 ± 0.5
Head in NRW	7.0*	1.81 ±0.02	----------	-3.57 ± 1.32	1.3 ± 0.5
CQD in D_2O	60.2 ± 0.5	5.04 ± 0.00	0.844	-30.13 ± 0.14	28.8 ± 0.1
CQD in NRW	60.2*	0.17 ± 0.01	0.17	-31.93 ± 0.50	22.9 ± 0.5
D_2O	Infinity	5.97 ± 0.00	----------	-30.69 ± 0.06	116.0 ± 0.3
NRW	Infinity	0.00 ± 0.00	----------	-21.95 ± 0.83	63.1 ± 1.9

t=thickness of the layer
ρ=Real part of the SLD
iρ=Imaginary part of the SLD
σ=roughness of the layer at the interface with the adjacent layer above it
ρ_{QD}= SLD of the QD layer
ρ_{SUB}= SLD of the subphase
Relative QD SLD= ρ_{QD}/ ρ_{SUB} (in case of D_2O subphase)
Relative QD SLD= ρ_{QD} - ρ_{SUB} (in case of NRW subphase)
*These values were fixed while fitting

Table S7: Fit parameters for the best fit of P1G1 + 10 nM CQD

Layer	**t (Å)**	**ρ (x 10^{-6} Å^{-2})**	**Relative QD SLD**	**iρ (x 10^{-14} Å^{-2})**	**σ (Å)**
Tail in D_2O	14.2 ± 0.1	5.19 ± 0.03	----------	-211.86 ± 0.93	6.0 ± 0.1
Tail in NRW	14.2*	4.88 ± 0.01	----------	-360.48 ± 0.82	3.9 ± 0.1
Head in D_2O	7.8 ± 0.1	3.16 ± 0.01	----------	-293.56 ± 1.48	1.9 ± 0.9
Head in NRW	7.8*	1.50 ± 0.01	----------	-174.83 ± 2.12	2.9 ± 0.2
CQD in D_2O	64.0 ± 0.4	5.02 ± 0.01	0.857	-9.87 ± 0.17	28.6 ± 0.1
CQD in NRW	64.0*	0.13 ± 0.00	0.13	-53.23 ± 0.48	16.6 ± 0.2
D_2O	Infinity	5.86 ± 0.00	----------	-22.84 ± 0.07	88.3 ± 0.4
NRW	Infinity	0.00 ± 0.00	----------	-42.69 ± 0.70	85.2 ± 2.7

t=thickness of the layer
ρ=Real part of the SLD
iρ=Imaginary part of the SLD
σ=roughness of the layer at the interface with the adjacent layer above it
ρ_{QD}= SLD of the QD layer
ρ_{SUB}= SLD of the subphase
Relative QD SLD= ρ_{QD}/ ρ_{SUB} (in case of D_2O subphase)
Relative QD SLD= ρ_{QD} - ρ_{SUB} (in case of NRW subphase)
*These values were fixed while fitting

Table S8: Parameters extracted out of NR fits of P1G1/5C and P1G1/10C

Sample	ϕ_{QD} (%)	$(\delta\rho)_t$ (%)	C_{SUB} (nM)
P1G1/5C	19.6 ± 1.2	-12.1 ± 0.2	5
P1G1/10C	17.9 ± 1.2	-4.8 ± 0.1	10

ϕ_{QD}= QD coverage

$(\delta\rho)_t$=Relative change in the SLD of the lipid tails (defined in text of the main manuscript)

The sample nomenclature has been explained in the main manuscript.

C_{SUB} is the concentration (in nM) of QDs injected into the subphase.

Fluorescence Microscopy:

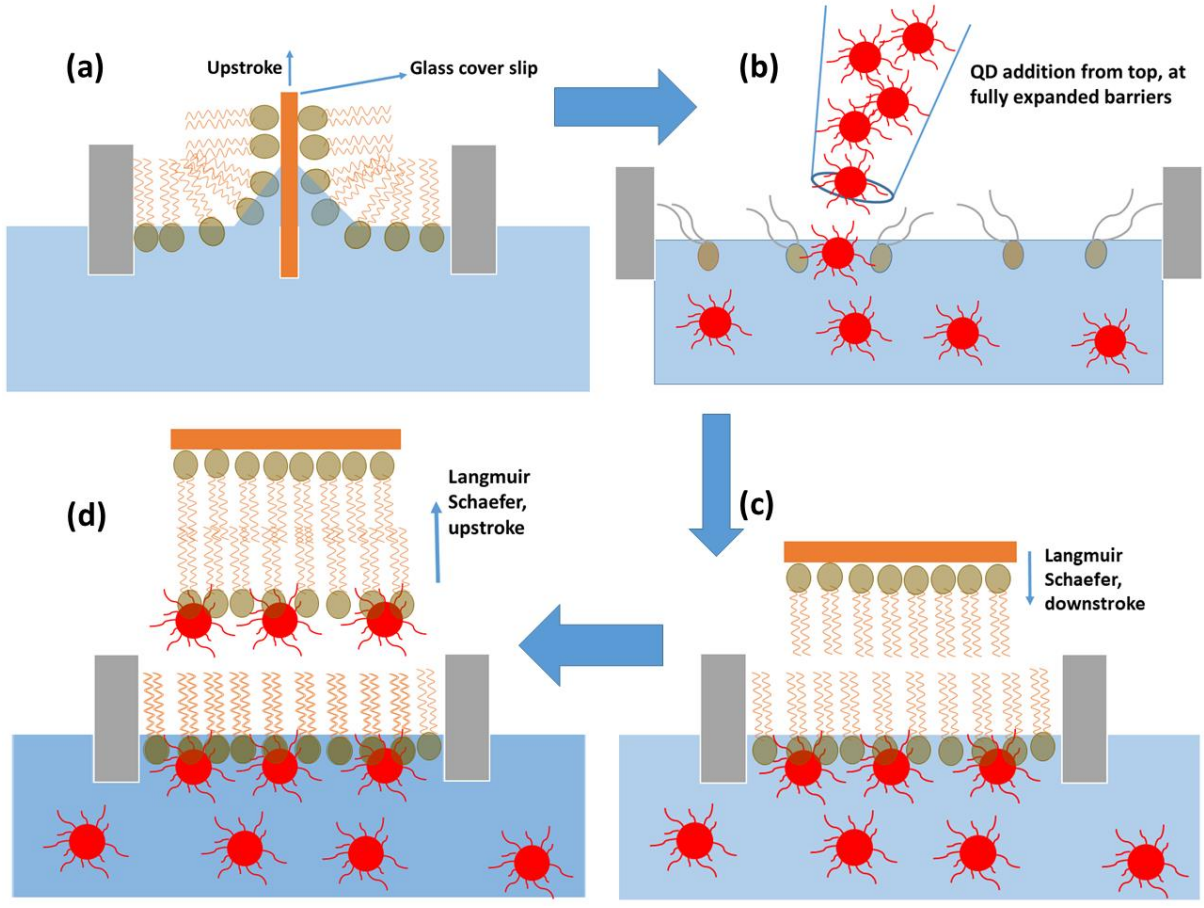

Fig S15: Schematic showing the transfer of QD bound supported lipid bilayers on glass substrates

Glass substrates of 0.017 ± 0.001 mm thickness, purchased from Glaswarenfabrik Karl Hecht GmbH & Co KG, Germany, were made hydrophilic by heating them in a solution of H_2O:NH_4OH:H_2O_2 =5:1:1 for 15 minutes at 80^0C, subsequently rinsing those with DI water thoroughly. The hydrophilic glass substrates were pre-inserted within the Langmuir trough filled with DI water subphase. These experiments were performed at a KSV NIMA setup at IISc, Bangalore, where a trough size of 243 cm^2 was used. A platinum Wilhemy was used as the sensor. To prepare a mixed FLM, individual lipids of 50 µl each, taken from their 1mM stock solutions, were mixed together. Using a Hamilton syringe, an aliquot of the mixture prepared in chloroform was spread on the water subphase for the formation of interfacial monolayer. It was left for 10-15 minutes to evaporate the chloroform from the air-water interface. The temperature of the trough was maintained at 20^0C using temperature-controlled chiller and water circulator provided by Srico Pvt. Ltd. Every FLM was subjected to one cycle of isothermal compression and expansion to distribute the film uniformly above the subphase. The FLM was finally compressed to 26 mN/m. Maintaining the surface pressure constant using barrier control, the pre-inserted glass was lifted above the subphase with an upstroke speed of 5 mm/min using the dipping apparatus (Fig. S15a). The trough was thoroughly cleaned and a mixed FLM of the same composition, also containing 10-20 µl of DMPE-conjugated Atto 647N (taken from a 20 µM stock solution), was spread over the buffered subphase (pH 7). After isothermal cycles of the FLM to homogenize the film, the barriers were fully expanded and the required concentration of the QDs were uniformly added from top throughout the trough area using a pipette (Fig. S15b). The supported lipid monolayer transferred to the glass cover slip was then stuck using a double-sided tape to an L-shaped Teflon holder attached to the dipping apparatus. The FLM with the added QDs was then compressed to the same area wherein the pristine FLM had attained a pressure of 26mN/m. With a downward stroke, the downward-facing hydrophobic film attached to the glass coverslip was made to adhere to the tails of the floating film, to which the QDs had been bound just beneath the air-water interface (Fig. S15c). Thereafter, with an upstroke, the QD-bound monolayer was made to attach to the supported pristine monolayer and the QD-bound membrane was lifted up (Fig. S15d). Thus, using Langmuir Schaefer technique, the QD-bound bilayers were deposited onto the glass substrates. All the microscopic and spectroscopic measurements on these bilayers were performed within one hour of transferring the films.

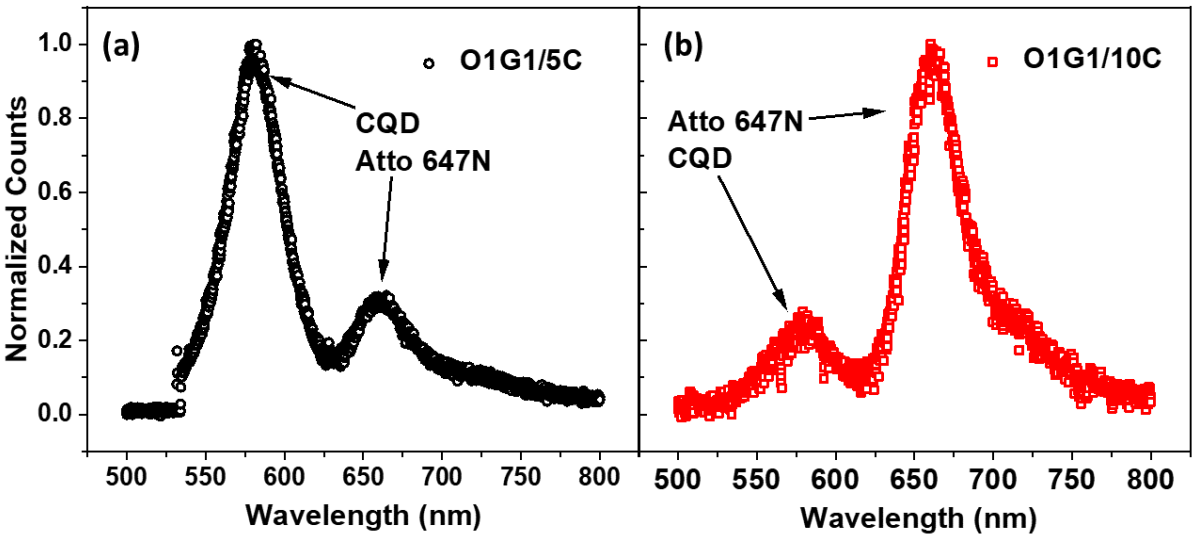

Fig. S16: PL spectra collected from (a) O1G1 + 5 nM CQD (O1G1/5C) and (b) O1G1 + 10 nM CQD (O1G1/10C) membranes. The two peaks arising due to fluorescence from CQDs and dmpe-conjugated Atto647N (lipid channel) have been labelled with arrows in the plots.

The Photoluminescence measurements were carried out in a Witec alpha300 R Microscopy setup. The glass substrates containing the QD-bound bilayers were placed at the imaging stage. The samples were optically excited with a PicoQuant 532 nm pulsed laser from top with 1 mW laser power. The laser beam was focussed using a 100x air objective and the fluorescence signal was collected from the same objective. The unwanted signal of the source 532 nm laser due to reflection from the substrate was filtered out using a notch filter. The signal was detected using a CCD detector.

Fig. S16 shows the spectra collected from O1G1/5C and O1G1/10C membranes. For O1G1/10C, the CQD fluorescence decreases which is due to unbinding, as discussed in the main article.

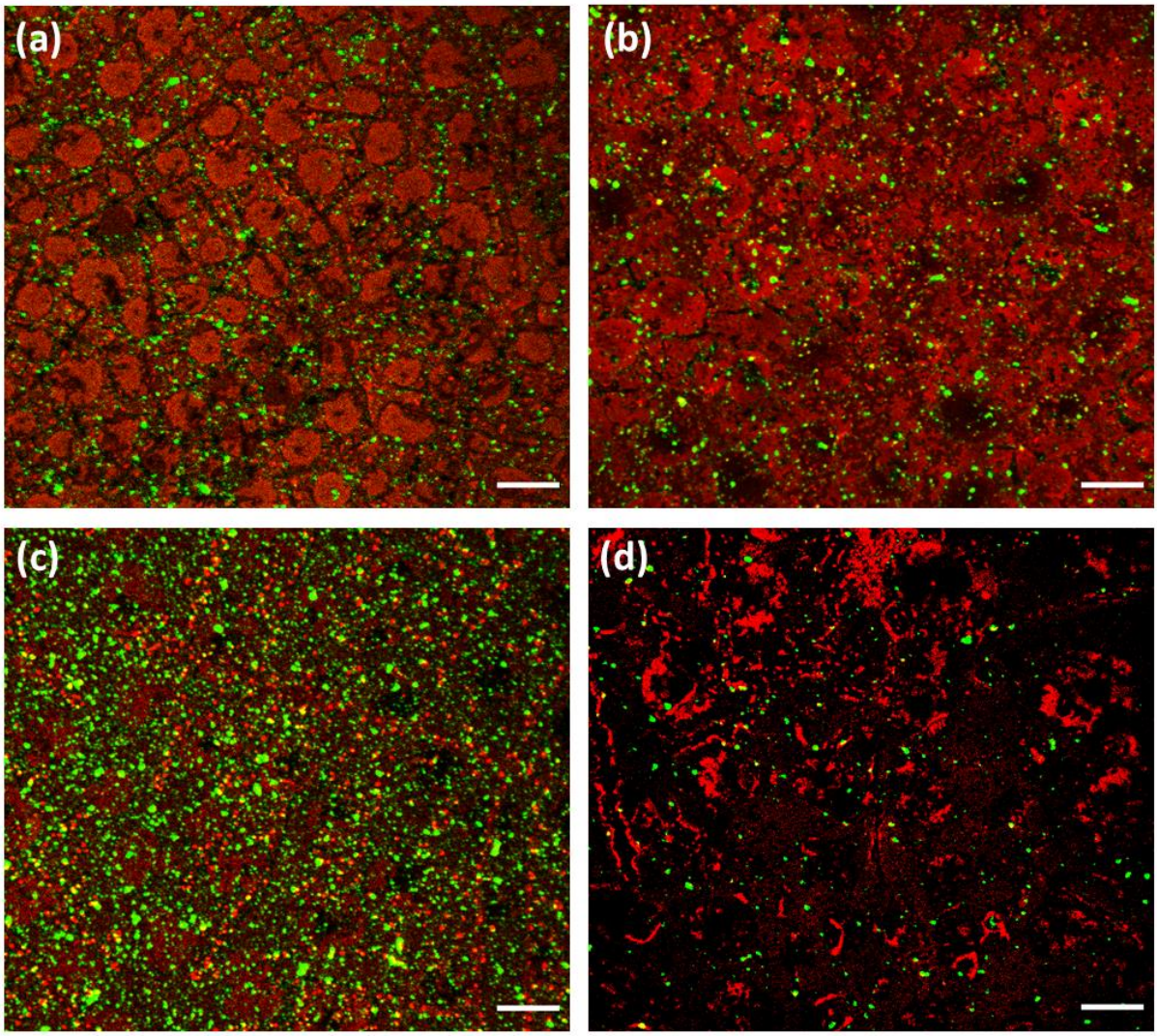

Fig S17: Fluorescence Microscopy co-localised images from (a) O1G1 + 5 nM ZQD (O1G1/5Z), (b) O1G1 + 10 nM ZQD (O1G1/10Z), (c) O1G1 + 20 nM ZQD (O1G1/20Z) and (d) O1G1 + 40 nM ZQD (O1G1/40Z) membranes. Red channel corresponds to the fluorescence from the lipid channel (tagged with dmpe-conjugated Atto 647N dye), while the green channel corresponds to the fluorescence from the membrane-bound ZQDs. The scale bar in each fluorescence image is 10 µm in length.

Fig. S17 shows the Fluorescence microscopic images of O1G1/5Z, O1G1/10Z, O1G1/20Z, O1G1/40Z samples. The imaging conditions has been mentioned in the Materials and Methods section of the main manuscript. As depicted in Fig. 5 of the main manuscript, the graph shows that the fluorescence from the membrane-bound ZQDs increases till 20 nM ZQD C_{SUB} (concentration in the subphase). In the membrane prepared by adding 40 nM ZQD in the subphase, the fluorescence from the bound ZQDs decreases, which is evident from Fig. S17d. The fluorescence from the Atto 647 dye (representative of the lipid content), decreases in the membrane which was prepared with ZQD C_{SUB} of 20 nM. This indicates lipid loss at this concentration.

The phenomenon of lipid loss along with loss of bound CQDs, which occurred for O1G1 membranes, was also observed in P1G1 membranes. The Fluorescence images in Fig. S18 and the quantified bar plot in the main manuscript Fig. 4i depict this process.

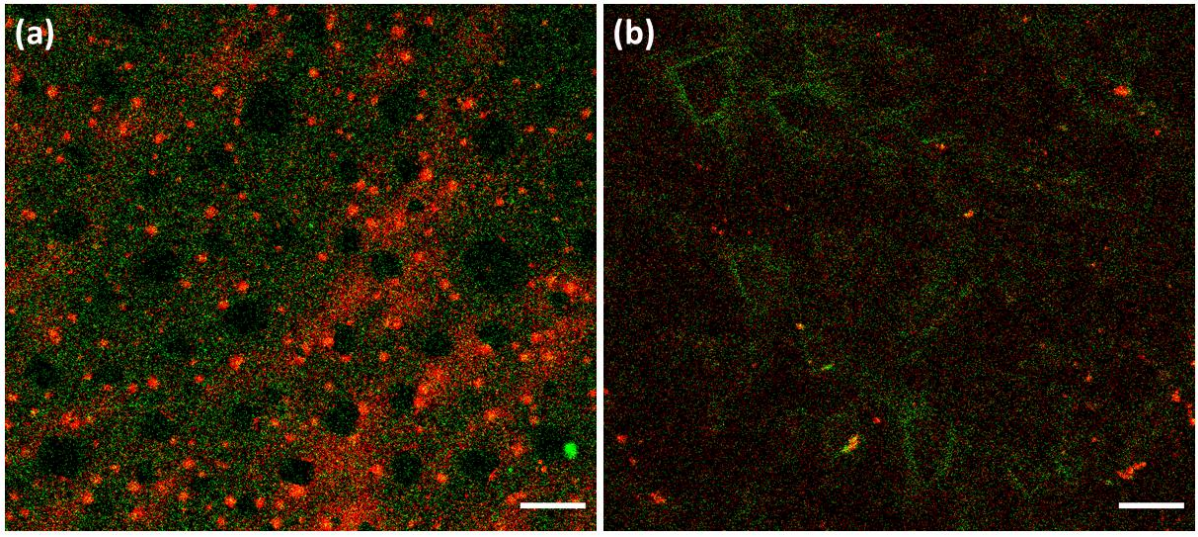

Fig S18: Fluorescence Microscopy co-localised images from (a) P1G1 + 5 nM CQD (O1G1/5C) and (b) P1G1 + 10 nM CQD (O1G1/10C) membranes. Red channel corresponds to the fluorescence from the lipid channel (tagged with dmpe-conjugated Atto 647N dye), while the green channel corresponds to the fluorescence from the membrane-bound CQDs. The scale bar in each fluorescence image is 10 µm in length.

References:

[1] S. J. Tan, N. R. Jana, S. Gao, P. K. Patra, J. Y. Ying, Surface-ligand-dependent cellular interaction, subcellular localization, and cytotoxicity of polymer-coated quantum dots, Chem. Mater. 22 (2010) 2239–2247.

[2] A. Saha, S. Basiruddin, R. Sarkar, N. Pradhan, N. R. Jana, Functionalized plasmonic- fluorescent nanoparticles for imaging and detection, J. Phys. Chem. C 113 (2009) 18492–18498.